

9/8/2006

Visible and Near-Infrared Spectrophotometry of the Deep Impact Ejecta of Comet 9P/Tempel 1

Klaus W. Hodapp^{a,*}, Greg Aldering^b, Karen J. Meech^c, Anita L. Cochran^d, Pierre Antilogus^h, Emmanuel Pécontalⁱ, William Chickering^b, Nathalie Blanc^j, Yannick Copin^j, David K. Lynch^e, Richard J. Rudy^e, S. Mazuk^e, Catherine C. Venturini^e, Richard C. Puetter^f, and Raleigh B. Perry^g

^aInstitute for Astronomy, University of Hawaii, 640 N. Aohoku Place, Hilo, HI 96720

*Corresponding Author E-mail address: hodapp@ifa.hawaii.edu

^bLawrence Berkeley Lab, Physics Div., MS-50/232, One Cyclotron Rd., Berkeley, CA 94720

^cInstitute for Astronomy, University of Hawaii, 2680 Woodlawn Drive, Honolulu, HI 96822

^dMcDonald Observatory, University of Texas at Austin, 1 University Station C1402,
Austin, TX 78712-0259

^eThe Aerospace Corporation, P.O. Box 92957, MS 266, Los Angeles, CA 90009

^fUniversity of California, San Diego, CASS 0424, 9500 Gilman Dr., La Jolla, CA 92093 San

Diego, CA

^gNASA Langley Research Center, MS 160, Science Support Office, Hampton, VA 23681

^hLaboratoire de Physique Nucléaire et des Hautes Energies IN2P3 - CNRS - Universités
Paris VI et Paris VII, 4 Place Jussieu Tour 33 - Rez des chaussée 75252 Paris Cedex 05

ⁱCentre de Recherche Astronomique de Lyon, 9, av. Charles André,
69561 Saint Genis Laval Cedex

^jInstitut de Physique Nucleéaire de Lyon, UMR5822, CNRS-IN2P3, Université Claude
Bernard Lyon 1, F-69622 Villeurbanne, France

Pages: 28

Tables: 1

Figures: 8

Proposed Running Head: Spectro-Photometry of Deep Impact

Editorial correspondence to:

Dr. Klaus W. Hodapp

Institute for Astronomy

640 N. Aohoku Place

Hilo, HI 96720

Phone: 808-932-2313

Fax: 808-933-0737

Email: hodapp@ifa.hawaii.edu

ABSTRACT

We have obtained optical spectrophotometry of the evolution of comet 9P/Tempel 1 after the impact of the Deep Impact probe, using the Supernova Integral Field Spectrograph (SNIFS) at the UH 2.2m telescope, as well as simultaneous optical and infrared spectra using the Lick Visible-to-Near-Infrared Imaging Spectrograph (VNIRIS) spectrograph. The spatial distribution and temporal evolution of the “violet band” CN (0-0) emission and of the 630 nm [OI] emission was studied. We found that CN emission centered on the nucleus increased in the two hours after impact, but that this CN emission was delayed compared to the light curve of dust-scattered sunlight. The CN emission also expanded faster than the cloud of scattering dust. The emission of [OI] at 630 nm rose similarly to the scattered light, but then remained nearly constant for several hours after impact. On the day following the impact, both CN and [OI] emission concentrated on the comet nucleus had returned nearly to pre-impact levels. We have also searched for differences in the scattering properties of the dust ejected by the impact compared to the dust released under normal conditions. Compared to the pre-impact state of the comet, we find evidence that the color of the comet was slightly bluer during the post-impact rise in brightness. Long after the impact, in the following nights, the comet colors returned to their pre-impact values. This can be explained by postulating a change to a smaller particle size distribution in the ejecta cloud, in agreement with the findings from mid-infrared observations, or by postulating a large fraction of clean ice particles, or by a combination of these two.

Key Words: Comets; 9P/Tempel 1; Deep Impact; Photometry; Spectroscopy

1. Introduction

As part of a coordinated simultaneous Earth-based observing campaign (Meech et al. 2005) of comet 9P/Tempel 1 before, during, and after the Deep Impact event, we used the Supernova Integral Field Spectrograph (SNIFS) (Aldering et al. 2002) to obtain spectral data cubes covering the wavelength range from 350 nm to 1000 nm. This data acquisition method ensured that spatial, spectral, and temporal information was obtained over a wide wavelength range, without having to pre-select specific filter bandpasses or slit orientations before the event. It was therefore very well suited for an event where a poorly understood range of phenomena was anticipated. We are also presenting data from the VNIRIS instrument at the Lick Observatory 3 m telescope. This instrument is a more conventional long-slit spectrograph and served to check our data at the limits of SNIFS' wavelength coverage. VNIRIS is a three-channel instrument with a wavelength coverage from 500 nm to 2200 nm and extended our wavelength coverage into the infrared.

After the impact event, it became clear that the most interesting aspects of our data were the spatial distribution and temporal evolution of the CN (0-0) emission at 388 nm and of the [OI] emission at 630 nm as well as the evolution of the continuum scattered light color in the hours after impact.

We will briefly describe the SNIFS instrument and the observing procedures and conditions in chapter 2. The data reduction steps used to extract specific information from the data cubes will be covered in chapter 3. Chapter 4 will discuss the results.

2. Observations

2.1. The Supernova Integral Field Spectrograph SNIFS

Comet 9P/Tempel 1 was observed in the nights of July 2 - 9, 2005 UT at the UH 2.2m telescope using the SNIFS spectrograph that is permanently mounted at the bent Cassegrain focus. The instrument is described in more detail by Aldering et al. (2002) and Lantz et al. (2004). The SNIFS instrument is designed to obtain photometrically calibrated spectra of supernovae against the background of their host galaxy. It is therefore well suited to obtain spectrophotometry of the gas and dust released from the comet nucleus by the impact of the Deep Impact probe against the background of the more extended coma.

Among the instruments used in the Earth-based Deep Impact observing campaign (Meech et al. 2005), SNIFS is unique in its capability to obtain photometrically calibrated spectral and spatial data over a very wide optical wavelength range.

SNIFS basically consists of a blue and a red spectrograph arm. After the two wavelength ranges are separated by a dichroic beamsplitter, the light in each arm is focused on a separate 15×15 lenslet array with $0.4''$ lenslets, forming a contiguous $6'' \times 6''$ field of view. Each lenslet produces an image of the telescope pupil, which then becomes effectively the entrance point into a grism spectrograph. Each of the 15×15 pupil images is dispersed and produces a spectrum on the CCD detector. The lenslet array is rotated at such an angle around the optical axis and against the orientation of the lenslet array that the 225 individual spectra do not overlap. The dispersion is 0.22 nm/pixel in the blue channel, the resolution is about 2 pixels, giving a resolving power of $\lambda/\Delta\lambda \approx 1000$ at 440 nm. The red channel has a dispersion of 0.29 nm/pixel and a resolving power of $\lambda/\Delta\lambda \approx 1300$ at 760 nm (Lantz et al., 2004). Spatially, one pixel of the extracted spectrum corresponds to one $0.4'' \times 0.4''$ lenslet element. The spectral resolution is not dependent on the image quality in

the telescope focal plane.

2.2. Observing Procedures and Conditions

Data were obtained on the nights of July 2 and 3 (UTC) prior to impact, on the night of July 4 (the impact night), when the first useful frame was exposed during the moment of impact, and on the nights of July 5, 7 and 8, after the impact. The nights of July 6 and 9 were lost due to a combination of poor seeing ($\approx 2''$) and cirrus clouds. The integration time used for comet spectra was 300 s on July 2 and 3, 90 s on July 4 and 5, and 180 s on July 7 and 8. The seeing in these nights was, of course, dependent on time, wavelength and air-mass. Typically, the FWHM of standard star frames was $\approx 0.7''$ in the red channel of SNIFS and $\approx 0.85''$ in the blue channel. The Deep Impact event was observed at a geocentric distance of 0.89 AU, resulting in a scale of $645 \text{ km arcsec}^{-1}$. The heliocentric distance was 1.51 AU.

Up to the night of July 7, the telescope was tracking the non-sidereal motion of comet Tempel 1 in open loop, without guiding. Keeping the comet nucleus centered in the field of view under these conditions proved rather difficult. We selected only those frames for analysis where the full photometric aperture was within the field of view, to avoid any possible color effects from extrapolating from smaller apertures. However, we were using frames where the photometric sky annulus was not fully contained in the field, a situation that the IRAF `apphot` package is designed to handle.

Observations of the comet were interdispersed with calibration observations, so that our coverage of the post-impact phase was not continuous. Observations of a position $5'$ away from the comet nucleus, outside of the comet's coma, were taken as "empty sky" frames and later used in the analysis of some of the data. Following the established procedures

for absolute photometric calibration of SNIFS data, solar analog stars with known absolute flux calibration were observed several times per night. Internal calibration data, a flat field exposure and a spectral lamp exposure, were also taken at every telescope position used for observations on the sky.

The night of July 4, 2005, UT, was photometric on Mauna Kea. The CFHT sky-probe data in the first half of that night were all taken in the vicinity of comet Tempel 1, since CFHT was also observing the Deep Impact event. We did not have the time during the impact event to determine the extinction independently. The nights of July 2, 5, 7, and 8 (UTC) were also photometric. The night of July 3 was not fully photometric, but usable.

2.3. Lick Observatory VNIRIS Observations

We are also presenting a spectrum obtained at the 3m telescope of Lick Observatory with the Visible and Near-Infrared Imaging Spectrograph (VNIRIS) to double-check our main conclusions and guard against artifacts introduced by the use of the innovative SNIFS instrument. The VNIRIS is a more conventional spectrograph than SNIFS. It has three long slit spectrograph channels, one optical channel, using a deep-depletion CCD, and two infrared channels. For the observations reported here, a slit width of $2.7''$ and nodding by $40''$ along the slit was used. The slit orientation was parallel to the parallactic angle to put atmospheric refraction along the slit. The integration on the post-impact ejecta cloud was centered on 6:42 UT (≈ 50 min post-impact) with a total integration time of 12 minutes, the air mass for the comet observations from Lick Observatory was about 3. A standard star (HD 126053) of spectral type G1V was observed as a solar analog star, but unfortunately not at exactly the same air mass.

3. Data Reduction

3.1. Spectral Datacube Extraction

The initial steps of the data reduction were done by the SNIFS data reduction pipeline (Aldering et al. 2002, Aldering et al. 2006). These steps were to remove instrumental artifacts from the CCD frames and to extract wavelength calibrated, extinction corrected and flux calibrated spectra for each of the 15×15 lenslets of the integral field units. Using bias frames, dark frames, continuum flatfields, and an arc lamp spectrum (He/Hg/Cd for the blue arm and Ne/Ar/Xe for the red arm), the CCD data were bias and dark-current corrected, were flatfielded, cosmic rays were removed, and the position of each lenslet spectrum and its wavelength calibration on the CCD frame was determined.

To calibrate the flexure effects in the instrument that are telescope-position dependent, at least one arc lamp frame was taken at essentially the same telescope position where a sequence of science data was taken. In the interest of observing efficiency during the impact time period, however, we did not take an arc calibration frame prior to every single exposure. As a result, the SNIFS real-time data reduction pipeline was run again after the completion of all the observations of the night so that the association of calibration frames to science frames could be optimized.

After extraction of each spectrum, the data were photometrically calibrated using flux calibrations derived from the observations of solar analog stars, including a standard extinction correction for clear photometric nights on Mauna Kea. The output of the SNIFS data reduction were cubes (x, y, λ) stored as Euro-3D FITS tables (Kissler-Patig et al. 2003), with x and y being the position of each individual lenslet in the integral field units.

3.2. Extraction of Spectral Images

From this state of the data reduction on, SNIFS usually reduces its supernova observations with a data reduction pipeline carefully tuned to the needs of the Nearby Supernova Factory project. While these pipeline data products were very useful for an initial inspection of the data from the Deep Impact observations, we decided for the final analysis of the data to bypass these photometric extraction functions of the SNIFS pipeline and instead to extract the photometric information directly from the Euro3D data cubes using IRAF (Tody, 1986) scripts. The main reason was to achieve better control of atmospheric dispersion in the extraction of broad-band spectrophotometry from the data cubes, better elimination of residual cosmic ray events in the data, and a better handling of the changing flux distribution over the course of the observations due to the expansion of the debris cloud around the comet.

Initially, the $15 \times 15 \times \lambda$ data cubes were processed into $225 \times \lambda$ two-dimensional spectra. In this format, the few residual cosmic ray events that had escaped automatic removal could be easily identified and interactively eliminated using the IRAF image editing task (imedit). As an example, Fig. 1 shows the extracted spectra in the blue and red channel in this two-dimensional format, which is essentially a set of 15 long (6'') slit spectra stacked in vertical direction. Note that for Fig. 1, we show a spectrum after subtraction of an “empty sky” frame taken a few minutes before the comet spectrum at a position 5' from the comet nucleus, outside of the coma. The sky subtraction was done to eliminate night sky emission lines from Fig. 1 which would otherwise limit the visibility of faint emission features in the comet’s coma. In this extracted, long-slit data format (Fig. 1), the CN (0-0) emission band at 388 nm is seen prominently. The C₃ emission band at 405 nm is also faintly indicated in the blue channel, but the signal-to-noise ratio is too low to analyze this emission in any more detail. The C₂ Swan bands were not clearly detected. The brightest C₂ band at

516 nm, in particular, lies in the overlap region of the blue and red SNIFS channels, where throughput is low and the resulting signal-to-noise ratio is poor. In the red spectrum the [OI] line at 630 nm is seen in the comet coma, and the red CN (1-0) band (911-932 nm) is faintly indicated in Fig. 1. This figure is a sky-subtracted spectrum, so telluric [OI] emission is removed to the degree that it is stable on timescales of a few minutes. Also, the line seen at 630 nm in Fig. 1 is clearly stronger near the comet nucleus than at the edge of the field of view, showing that it originates in the comet. However, it should be noted that for the extraction of spectrophotometric information by aperture photometry that we will describe later, we did not subtract a separate sky frame, since the sky subtraction was done as part of the aperture photometry procedure by measuring the “sky annulus” around the object on the object frame itself.

An extracted sky-subtracted spectrum of the comet near the time of maximum post-impact continuum flux (one half hour after impact) in a 2.4'' (6 pixel) diameter aperture is shown in Fig. 2. This spectrum is a reflectivity spectrum, obtained by dividing the comet spectrum by a spectrum of a solar analog star. The blue and red channel of SNIFS were joined at 520 nm, relying purely on the instrumental flux calibration without any further adjustments. In Fig. 2, we also plot (as small symbols) data from both the blue and red arm of SNIFS that we do not consider reliable. In both channels of the SNIFS spectrograph, the data points at the short and long wavelength end of their respective range lie below the extrapolated spectrum, and in the case of the overlap region around 520 nm, lie mostly below the other channel. The seamless transition between the two spectrograph arms illustrates the reliability of the instrumental calibration in that transition region. The spectrum shows the violet emission band of CN, the C₃ band, and the emission line of [OI]. The feature at 763 nm is an artifact from improper correction of the telluric O₂ absorption, the strongest atmospheric absorption feature in the spectral range of our observations.

For comparison, the extracted VNIRIS spectrum is shown in Fig. 3. The slit width was $2.7''$ and the extraction along the slit was limited to the profile of the unresolved ejecta cloud at the time of the observations. Therefore, the spectrum in Fig. 3 is dominated by the unresolved ejecta cloud and the extended emission from the coma is strongly suppressed. Also, by comparison with the VNIRIS spectrum, it is clear that the drop in signal at the longest wavelength end (between 950 and 1000 nm) in the SNIFS spectrum is not real. The VNIRIS spectrum shows a feature at ≈ 920 nm from improper correction of a telluric H_2O absorption feature, but this is distinct from the feature seen in the SNIFS data. This absorption feature is much more pronounced in the VNIRIS data due to the high airmass of the observations, the difference in airmass between object and standard, and the relatively low elevation of the Lick Observatory site.

Both for the extraction of emission band fluxes and for broad-band continuum photometry, spectral images were extracted from the data cubes by integrating over the selected wavelength range and by arranging the spatial dimensions into the proper orientation. Examples of these small $6'' \times 6''$ images are shown in Figs. 4 and 5.

3.3. Aperture Photometry

Aperture photometry was obtained with the IRAF `apphot` package. The aperture photometry signal is the sum of the flux of all pixels fully contained in the “object aperture”, minus an estimate of the “sky” flux interpolated from the average flux in a surrounding “sky annulus”. In the specific case of comet observations, the “sky annulus” also contains flux from the comet coma, which consequently gets subtracted from the flux in the aperture. Therefore, our aperture photometry is sensitive only to flux concentrated in the small photometry aperture, and not to more extended flux. This characteristic of the aperture photometry leads to the sharp flux maximum and subsequent rapid decline

of continuum and CN aperture photometry in Fig. 6. The aperture photometry software treats fractional pixels in the integration aperture properly, a feature important for the small images and relatively coarsely sampled ($0.4''$) data obtained by SNIFS. Also, *apphot* generates error messages when the integration aperture exceeds the frame boundaries, but works in conditions where the sky annulus exceeds the frame boundaries, not an infrequent occurrence on the small SNIFS frames.

3.4. Emission Band Images

3.4.1. *CN Emission*

The emission of the CN (0-0) band is the highest signal-to-noise emission feature in our data and allows a detailed study of its temporal and spatial evolution. Spectrophotometric information was extracted in a 10 pixel (2.9 nm) wide spectral window that included all the flux from the CN band. The adjacent continuum was measured in two windows of the same size, at the adjacent shorter and longer wavelengths. Since the solar scattered light contains numerous absorption lines in this wavelength range, we divided the 2-dimensional comet spectrum by the spectrum of solar analog star P041C, normalized to unity signal at the center of the bandpass used to extract the CN emission (Colina and Bohlin 1997, and Bohlin, Dickinson, and Calzetti 2001). The underlying continuum spectrum, normalized by the solar analog spectrum, was then estimated by the average of the two adjacent continuum wavelength intervals and subtracted from the spectral interval containing the CN emission. The resulting continuum-subtracted CN emission spectral frame was averaged in wavelength and rearranged into a spatial image of the CN flux distribution.

Information on the CN flux was extracted from this continuum subtracted CN emission image in two complementary ways: First, the average flux over the full $6'' \times 6''$ field of

view was computed using the IRAF task “imstat”. This gives, in essence, the surface brightness of CN emission in the inner coma of comet Tempel 1, since the CN emission extends beyond the limits of our field of view. The varying centering of the comet coma in our images injects some additional noise even in these field-averaged data, but for times before and long after the impact, when CN was much more extended than our $6'' \times 6''$ field of view, the data are reliable. Second, we obtained aperture photometry with an object aperture diameter of 7 pixels ($2.8'' = 1800$ km) and sky annulus between $3.2''$ and $4.8''$ diameter. The CN photometry aperture was centered on the flux in the 350 nm - 400 nm integrated image, which was dominated by scattered continuum light and had enough signal-to-noise for reliable centroid computation. This procedure avoided the problem that the “apphot” centering algorithm might otherwise peak up on random noise spikes in the low signal-to-noise CN image. By using a continuum wavelength range that included the wavelength of the CN emission, effects of differential atmospheric refraction on the position of the extraction aperture were avoided. The 350 - 400 nm continuum images and a median-filtered version of the CN emission images are shown in Fig. 4 and both the CN flux averages and aperture photometry are included in Fig. 6. Note that the median filtering of the CN images was done only for clarity in Fig. 4. The photometry was extracted from the unfiltered CN images.

3.4.2. *[OI] Emission*

The [OI] emission at 630 nm was extracted over a wavelength range of 0.9 nm (3 pixels) centered on the line, and the continuum was measured by interpolation between adjacent continuum bands, and then subtracted. In the same way as for the CN emission, the comet spectra were divided by a normalized spectrum of the solar analog star P041C prior to the extraction of the line emission. The 3.5 pixel radius ($2.8''$ diameter) photometric

aperture was centered on the centroid of the 600 - 650 nm continuum spectral image. The comparison of 600 - 650 nm continuum and the continuum-subtracted [OI] flux is shown in the sequence of images in Fig. 5. The sky-annulus subtraction used as part of the aperture photometry eliminated any contribution of telluric [OI] emission. The aperture photometry of [OI] emission is included in Fig. 6 as filled circles.

3.5. Broad-band Aperture Photometry

The spectral data cubes were integrated over the bandpasses listed in Table 1. The bandpasses cover the whole spectrum from 350 nm to 950 nm, with the exception of a gap at $\lambda \approx 525$ nm, in the beamsplitter transition region between the blue and red arm of the SNIFS instrument. Also, the region of heavy telluric O₂ absorption at ≈ 763 nm was avoided. The data integrated over the bandpass were rearranged as a set of 2-dimensional synthetic bandpass images. Aperture photometry using the IRAF “apphot” package with an integrating aperture of 2.4'' (1550 km) diameter was then performed. The SNIFS data are recorded in separate blue and red arms of the spectrograph. The boresight of these two arms are not precisely identical. In addition, for observations at higher airmass, atmospheric dispersion leads to a wavelength dependence of the centroid position, as is evident by a comparison of the images obtained in blue (Fig. 4) and red (Fig. 5) bandpasses. Therefore, for the continuum photometry of comet 9P/Tempel 1, we centered the photometry aperture individually on each bandpass image.

The data are presented in Figs. 7a and 7b as instrumental magnitudes, so that changes in brightness lead to a linear shift of the spectral distribution. All data are normalized to the flux distribution of the Sun. To do this normalization, a solar analog star, P041C, was observed several times during the night of July 4, 2005, (UTC). As discussed by Colina and Bohlin (1997) and Bohlin, Dickinson, and Calzetti (2001), P041C has an effective

temperature of 5900 K, slightly higher than that of the Sun (5777K). The flux ratio of P041C to the Sun is given by Bohlin, Dickinson, and Calzetti (2001) and our measured spectrophotometry was corrected accordingly. All data in Figs. 7a and 7b are normalized to this corrected P041C flux by subtracting the corrected average instrumental magnitudes of P041C, and therefore represent a normalization to the solar flux distribution. In Fig. 7a and 7b, we show the solar analog standard stars observed on three nights in the same normalization. The data on P041C show a slightly blue spectrum in Figs. 7a and 7b, while the spectral energy distribution of P177D shows small excesses both at short and long wavelengths, both consistent with the results by Colina and Bohlin (1997). This good agreement in the colors of the standard stars gives us confidence that the spectrophotometric calibration of the SNIFS instrument is stable over the observing period. The observed changes in the spectrophotometry of comet Tempel 1 in the hours after impact are therefore considered real.

The photometric errors were estimated from repeated observations of the comet on July 5, 2005 (UTC), i.e., after the rapid changes in brightness induced by the impact had subsided. The largest error comes from changes in the image quality due to seeing changes, focus drifts, and tracking errors and affect all wavelengths in nearly the same way, and possibly also from intrinsic changes in brightness of the comet. For the estimation of uncorrelated photometric errors, the photometric data were normalized to the same magnitude average over the 625 - 825 nm range, where the signal to noise ratio was highest. The rms scatter of the photometric values after this normalization of the average flux is represented by the error bars shown in Figs. 7a and 7b. These error bars are characteristic of the photometric errors when the comet was at or near its pre-impact brightness, and also in the days after the impact when the nucleus and inner coma had returned practically to pre-impact levels. While the comet was near its maximum brightness post-impact, and even more so for the standard stars, the uncorrelated photometric errors were smaller than

the data point symbol in Figs. 7a and 7b.

4. Discussion

4.1. Gas emission

The formation and excitation of CN and [OI] emission is discussed in detail in Manfroid et al. (2006) in this issue of *Icarus*. The timescale for the creation of the CN radical from its grandparent and parent molecules under normal steady-state conditions is long compared with the duration of the July 4 post-impact observations. Haser model lifetimes for the parent of CN are of order 3×10^4 s (Schleicher and Farnham 2004). The lifetime of the daughter against photodissociation is 2×10^5 s. However, the typical lifetime is the e-folding lifetime for dissociation. Some amount of gas is produced earlier, while other is produced later than this time. Under normal, steady-state conditions, it is difficult to see gas with a timescale different than the average. However, the Deep Impact event was very distinct from steady state so that the impulse in CN production can be seen in many data sets obtained of this event (e.g. Cochran, Jackson, Meech and Glaz 2006).

On the other hand [OI] is a prompt emission, meaning that OI is directly being produced in its excited states by photodissociation of one of its many possible parent molecules (H_2 , OH, CO_2 , or CO). The ^1D state responsible for the 630 nm emission has a lifetime of ≈ 110 s. The 630 nm [OI] emission line is therefore spatially closely coupled to the location of the parent molecules and should increase in proportion to the prevalence of the parent molecule.

4.1.1. Temporal Evolution of CN Emission

Fig. 4 shows a median filtered version of the input data for this CN photometry. In Fig. 6 the resulting CN aperture fluxes are shown as open triangles.

Our last exposure of the first set of images (top row in Fig. 4) ended at 06:07:25 (UTC) and did not yet show centrally concentrated CN emission. Our data first recorded centrally concentrated CN emission in the exposure centered at 06:23:28 (UTC). Observations at the Keck telescope by Cochran et al. (2006) show the first sign of CN emission in an exposure lasting from 06:06:12 to 06:16:12 (UTC). These data are consistent if we assume that most of the CN flux in the Keck frame was collected later in the exposure time, after 06:07:25 (UTC). In combination, these data indicate that centrally concentrated CN emission became detectable ≈ 20 minutes after the impact. The CN lightcurve therefore trails the 350 - 400 nm integrated light curve (open stars in Fig. 6.) that began to rise immediately after the impact.

In Fig. 4, we also show the CN images obtained in the minutes before impact, even though they were not centered well on the comet. While aperture photometry on these images was not possible and while the noise was elevated due to the twilight sky brightness, we show them here for completeness. The image taken at the time of impact (mid-exposure at 05:52:37 UTC) shows a weak feature near, but not precisely at the position of the comet. Because of the discrepancy of the centroid positions, we conclude that the feature in this image is an artifact, and not a detection of the impact flash. Despite the position discrepancy, the aperture photometry shows an elevated value for this image, which, by the same argument, we also consider spurious, despite its formal 3σ significance.

The signal average and standard deviation in the measurements in the night of July 7 and 8, after the rapid changes have subsided are $1.6 \pm 173 \times 10^{-20} \text{ Wm}^{-2}$, i.e. the CN aperture photometry signal is zero. For the shorter 90s exposure times used on July 4, the

noise would be expected to be $245 \times 10^{-20} \text{ Wm}^{-2} \text{ rms}$. Therefore, the detections of elevated flux levels in the hours after impact are significant at above the 3σ level.

At the end of the observations on July 4, (UTC), about 3 hours after impact, the CN emission had spread beyond the full field of view and the central concentration of CN emission had disappeared. Therefore, the CN flux in the aperture and in the sky annulus were at the same level and the aperture photometry signal consequently had returned to zero. The average CN emission over the full $6'' \times 6''$ field, however, peaked about 2 hours after impact, just at the time when the impact-generated emission began to fill the field of view. It declined slowly thereafter, as the impact-generated emission expanded beyond our field of view and flux therefore got lost.

The CN images in Fig. 4 have very low signal-to-noise ratio and do not allow a very precise measurement of the CN expansion velocity. Under the reasonable assumption that during the middle set of images in Fig. 4, roughly at 07:40 (UTC), ≈ 108 minutes after impact, the CN had reached the corner of the image farthest from the comet (about $6'' \approx 3870 \text{ km}$), we get an average projected expansion velocity for CN and its parent molecule of 0.6 km/s , in rough agreement with the measurement at Keck by Cochran et al. (2006).

On the night of July 5, 2005, the night following the impact, the average CN emission flux had stabilized to a level slightly higher (12%) than prior to impact, and remained at that level on the nights of July 7 and 8. The average of all integrated CN flux measurements in the nights of July 2 and 3, in units of 10^{-20} Wm^{-2} in Fig. 6, and scaled to a $2.8''$ aperture, is 2202, with a standard deviation of 92. The standard error of the average of 7 measurements is therefore 35. In the nights of July 5, 7, and 8, the average of 15 measurements is 2473 with a standard deviation of 69 and a standard error of the average of 18. The change in CN flux average is therefore statistically significant. Since we used an instrument specifically designed for spectrophotometry and since we used this instrument

continually through the Deep Impact observing campaign under stable sky conditions, we are confident that we are not seeing systematic changes in the instrument characteristics. We therefore believe that the 12% change in CN flux integrated over our field of view is real. It is not clear whether the small increase in CN parent molecular release was caused by the impact, or whether the change in CN production happened independently of the impact. No concentration of the CN flux centered on the nucleus was found on the nights prior to and after the impact night. We did not find any indication for periodic variations in the integrated CN flux with the rotation of the comet nucleus. Such variations were claimed by Jehin et al. (2006). None of our observations 2 day and 1 day prior to impact, and 1 day, 3 days, and 4 days after impact would have included the maximum phase of their reported periodic variations occurring 1.6 days prior and 0.1 day, 1.8 days, and 3.5 days after impact. Therefore, our data can neither support nor contradict their finding.

4.1.2. Temporal Evolution of [OI] Emission

The [OI] flux follows the lightcurve of the broad-band flux quite closely. Prior to the impact and in the days long after the impact, the [OI] flux concentrated on the comet nucleus is detectable in our aperture photometry. The standard deviation of individual photometric measurements on July 5 is $96 \times 10^{-20} \text{ Wm}^{-2}$ at an integration time of 90 s. The uncertainty of individual measurements on July 4, where the signal changed rapidly, should be the same. Therefore, the detection and the changes detected are significant above the 5σ level. Post impact, on July 5, individual data points detect [OI] flux in the aperture at the 3σ level. Assuming that the flux in this night was constant over timescales of about half hour so that the scatter of the measurements represents noise, the standard error of the average flux in this night is a 6σ detection. Due to the longer integration time of 180 s, the standard deviation in the nights of July 7 and 8 is only ≈ 60 , leading to a 6σ level of

confidence in the flux averages in those nights.

In the first hour after impact, the [OI] flux rises by about a factor of 3, and then slowly declines after peak flux in the aperture was reached 45 minutes after impact. The decline in flux is slower than that of CN flux and of blue broad-band continuum flux. In the night following the impact [OI] flux in the photometry aperture is down to less than half of the peak flux, but still appears somewhat elevated above the level seen before impact, even though this statement is uncertain due to the poor signal-to-noise of the data. Three and four nights after the impact, the [OI] flux in the aperture is indistinguishable from that before the impact. Spatially, the [OI] flux expands in unison with the continuum, and much slower than the CN flux.

CN is probably a daughter species of a yet unidentified parent molecule, whereas [OI] is both a daughter and a granddaughter of H_2O and can also be produced from other parents. Dissociation of H_2O (and other parent molecules) produces OI in its excited state of short lifetime and the [OI] emission therefore traces the presence of the parent closely. Additionally, the impact released a great deal of large H_2O ice particles which had a slower outflow velocity than the gas and subsequently fragmented, with some producing [OI]. This more complicated combined production and close link to the presence of H_2O ice and gas can account for the different scale lengths of [OI] when compared with CN and for the different temporal evolution of the [OI] flux.

4.2. Continuum Spectrophotometry

4.2.1. Reflectance Spectrum

Overall, the spectrophotometry of comet Tempel 1 both before and after the impact indicates a red color of the scattered light, similar to that found in most comets. In the

logarithmic presentation (magnitudes) chosen in Fig. 7a and 7b for the spectrophotometry, as well as in the linear plot in Fig. 2 and 3, we see a steepening of the spectral energy distribution at the shortest wavelengths. In many comets, this region is dominated by gas emission (CN, C₃, and C₂). By avoiding the emission features, as was done in our aperture photometry, or in comets with intrinsically low outgassing, evidence for a steeper slope of the reflectivity spectrum at short wavelengths is evident, for example in Jewitt & Meech (1986). Outside of the emission and absorption features, the reflectivity of the ejecta cloud after the Deep Impact event in the SNIFS observations can be roughly described by two linear fits. From 350 nm to ≈ 580 nm, the normalized reflectivity gradient as defined by Jewitt & Meech (1986) is $\approx 22.6\%$ per 100 nm. From 580 nm to 940 nm, it is $\approx 7.5\%$ per 100 nm. The two lines corresponding to these fits are included in Fig. 2. It is noteworthy that the break between these two slopes does not coincide with the wavelength break between the blue and red channel of the SNIFS instrument at 520 nm, and is therefore considered real. Similarly, the VNIRIS spectrum is steeper at the short wavelength end, even though the break is less pronounced than in the SNIFS spectrum. We suggest that the small differences between these two spectra reflect residual calibration problems. The trend towards a flatter reflectivity spectrum continues into the infrared, the spectrum measured by VNIRIS is almost flat between 1500 nm and 2200 nm.

4.2.2. Changes in Scattering Properties after Impact

All the spectrophotometric data obtained while the photometry aperture was dominated by impact ejected material show that this material had a bluer reflectivity spectrum than the material usually released by the comet. The dotted line in Fig. 7a and 7b fitted to all photometric data points is the average flux distribution in the data set taken about one half hour after impact, when the ejecta cloud was still nearly unresolved and at

its maximum brightness. The average post-impact maximum-light spectral distribution is shifted to match the average flux from 625 nm to 875 nm at other times. The deviations from this fits at times prior to the impact, and in the days after the impact when the inner coma of comet Tempel 1 had essentially returned to its normal condition, show that the flux at short wavelenths was lower at those times. The 375 nm data point is about 0.2 mag lower than during the peak post-impact brightness. This is particularly well seen in the 7/5, 7/7, and 7/8 data points in Fig. 7b. For the quiescent state of the comet, the long wavelength points lie systematically above the fitted impact ejecta spectrum, the effect is small (≈ 0.05 mag). Over the full range from 375 nm to 925 nm, we observe that the impact generated ejecta were ≈ 0.25 mag bluer than the quiescent comet coma. This corresponds to a $\approx 4\%$ per 100 nm change in the slope of the spectrum averaged over the wavelength range from 375 nm to 925 nm.

This change in color can be explained by an unspecific combination of two effects. First, the particle size distribution of the material ejected after the impact may contain a larger fraction of very small particles, much smaller than the wavelengths of visible light that leads to a bluer color of the Raleigh scattered light. Second, it may point to large quantities of pure water ice crystals that are known to have blue optical reflection spectra (Lucey & Clark 1985). Infrared observations of the post-impact material have also found indications that the size distribution of impact-ejected material contained more small particles than were released by the comet outside of the impact event (Harker Woodward and Wooden 2005) and (Sugita et al. 2005).

In combination, the changes in the comet's color in the hours after impact indicate that the material ejected by the impact contains smaller particles and more ice, and is therefore probably more pristine than the material released from the surface of the comet under normal conditions.

5. Conclusions

Our spectrophotometric observations of comet 9P/Tempel 1 in the days prior, during, and after the impact of the Deep Impact probe allow the following conclusions:

1. The impact ejecta contained the parent molecule for the CN radical. A noticeable level of CN emission centered on the newly created ejecta cloud was first found twenty minutes after impact, while the maximum CN flux in our field of view was measured about 2 hours after impact.

2. In the night following the Deep Impact, the CN emission integrated over our field of view had returned to a level about 12% higher than pre-impact. The CN emission then remained constant at this level 3 and 4 days after the impact.

3. Emission in the [OI] line at 630 nm increased in the first one hour after impact, and then levelled off to a nearly constant value for the next few hours. One day after the impact, [OI] emission had gone back to the pre-impact levels.

4. The impact ejecta contained, or soon fragmented into, a dust particle size distribution with a larger fraction of small particles than the material normally released by the comet. As a result, the spectrophotometry during the impact shows the scattered light from the expanding ejecta cloud with slightly bluer color than the normal coma of the comet.

5. The reflectivity spectrum of comet Tempel 1 before, soon after, and long after the impact shows a steeper slope at $\lambda < 600$ nm than at longer wavelengths. The reflectivity spectrum at infrared wavelengths is essentially flat.

Acknowledgments This project was in part supported the The Aerospace Corporation's Independent Research and Development Program.

References

- Aldering, G., Adam, G., Antilogus, P., Astier, P., Bacon, R., Bongard, S., Bonnaud, C., Copin, Y., Hardin, D., Henault, F., Howell, D. A., Lemonnier, J.-P., Levy, J.-M., Loken, S. C., Nugent, P. E., Pain, R., Pecontal, A., Pecontal, E., Permuter, S., Quimby, R. M., Schahmaneche, K., Smadja, G., Wood-Vasey, W. M. 2002.
- Overview of the Nearby Supernova Factory.
- Proc. of the SPIE, Volume 4836, 61-72.
- Aldering, G., Antilogus, P., Bailey, S., Baltay, C., Bauer, A., Blanc, N., Bongard, S., Copin, Y., Gangler, E., Gilles, S., Kessler, R., Kocevski, D., Lee, B. C., Loken, S., Nugent, P., Pain, R., Pecontal, E., Pereira, R., Perlmutter, S., Rabinowitz, D., Rigaudier, G., Scalzo, R., Smadja, G., Thomas, R. C., Wang, L., and Weaver, B. A. 2006.
- Nearby Supernova Factory Observations of SN 2005gj: Another Type Ia Supernova in a Massive Circumstellar Envelope.
- ApJ, in press, available on astro-ph 0606499.
- Bohlin, R. C., Dickinson, M. E., and Calzetti, D. 2001.
- Spectrophotometric Standards from the Far-Ultraviolet to the Near-Infrared: STIS and NICMOS Fluxes.
- The Astronomical Journal, 122, 2118-2128.
- Cochran, A. L., Jackson, W. M., Meech, K. J., Glaz, M. 2006.
- Observations of Comet 9P/Tempel 1 with the Keck 1 HIRES Instrument during Deep Impact.
- Icarus, submitted, this issue.
- Colina, L., Bohlin, R. 1997.
- Absolute flux distributions of solar analogs from the UV to the near-IR.

The Astronomical Journal 113, 1138-1144.

Feldman, P. D., Cochran A. L. and Combi, M. R. "Spectroscopic Investigations of Fragment Species in the Coma" in Comets II pp. 425-448 Comets II is edited by Festou, M. C., Keller. H. U. and Weaver H. A. The University of Arizona Press, Tucson 2004

Fink, U., Hicks, M. D. 1996.

A survey of 39 comets using CCD spectroscopy.

ApJ459, 729-743.

Harker, D. E., Woodward, C. E., Wooden, D. H. 2005.

The dust grains from 9P/Tempel 1 before and after the encounter with Deep Impact.
Science 310, 278-280.

Jehin, E., Manfroid, J, Hutsemékers, D, Cochran, A. L., Arpigny, C., Jackson, W. M.,
Rauer, H., Schulz, R., Zucconi, J.-M. 2006.
Astrophysical Journal, in press.

Jewitt, D., Meech, K. J. 1986.

Cometary grain scattering versus wavelength, or, "What color is comet dust?"
The Astrophysical Journal 310, 937-952.

Kissler-Patig, M., Copin, Y., Ferruit, P., Pécontal-Rousset, A., Roth, M. M. 2003
"The Euro3D data format: A common FITS data format for integral field spectrographs"
Astronomical Notes 325, 159-162.

Lantz, B., Aldering, G., Antilogus, P., Bonnaud, C., Capoani, L., Castera, A., Copin, Y.,
Dubet, D., Gangler, E., Hénault, F., Lemonnier, J.-P., Pain, R., Pécontal, A., Pécontal, E.,
Smadja, G. 2004.

SNIFS: a wideband integral field spectrograph with microlens arrays.

Proc. of the SPIE, Volume 5249, 146.

Lucey, P. G., Clark, R. N. 1985.

Spectral properties of water ice and contaminants

NATO ASI series, V. 156, Proc. NATO Advanced Research Workshop on Ices in the Solar System

Reidel, Dordrecht, p. 155-168.

The Astrophysical Journal 310, 937-952.

Manfroid, J., Hutsemékers, Jehin, E., Cochran, A. L., Arpigny, C., Jackson, W. M., Meech, K. J., Schulz, R., Zucconi, J.-M. 2006,

The impact and rotational lightcurves of Comet 9P/Tempel 1.

Icarus, in press, astro-ph 0608611.

Meech, K. J., and 208 colleagues 2005.

Deep Impact: Observations from a Worldwide Earth-Based Campaign.

Science 310, 265-269.

Sugita, S., Ootsubo, T., Kadono, T., Honda, M., Sako, S., Miyata, T., Sakon, I., Yamashita, T., Kawakita, H., Fujiwara, H., Fujiyoshi, T., Takato, N., Fuse, T., Watanabe, J., Furusho, R., Hasegawa, S., Kasuga, T., Sekiguchi, T., Kinoshita, D., Meech, K. J., Wooden, D. H., Ip, W. H., A'Hearn, M. F. 2005.

Subaru Telescope Observations of Deep Impact.

Science 310, 274-277.

Tody, D. 1986.

“The IRAF Data Reduction and Analysis System”,

SPIE Instrumentation in Astronomy VI, Ed. D. L. Crawford, 627, 733-748.

Schleicher, D. G. and Farnham, T. L. "Photometry and Imaging of the Coma with Narrowband Filters" in Comets II pp. 449-470 Comets II is edited by Festou, M. C., Keller.

H. U. and Weaver H. A. The University of Arizona Press, Tucson 2004

Table 1. Spectrophotometry Spectral Bins

Bandpass	λ_1	λ_2
	[nm]	[nm]
375	350	400
425	400	450
475	450	500
575	550	600
625	600	650
675	650	700
725	700	750
815	780	850
875	850	900
925	900	950

Figure 1, Hodapp et al., Deep Impact Spectro-Photometry

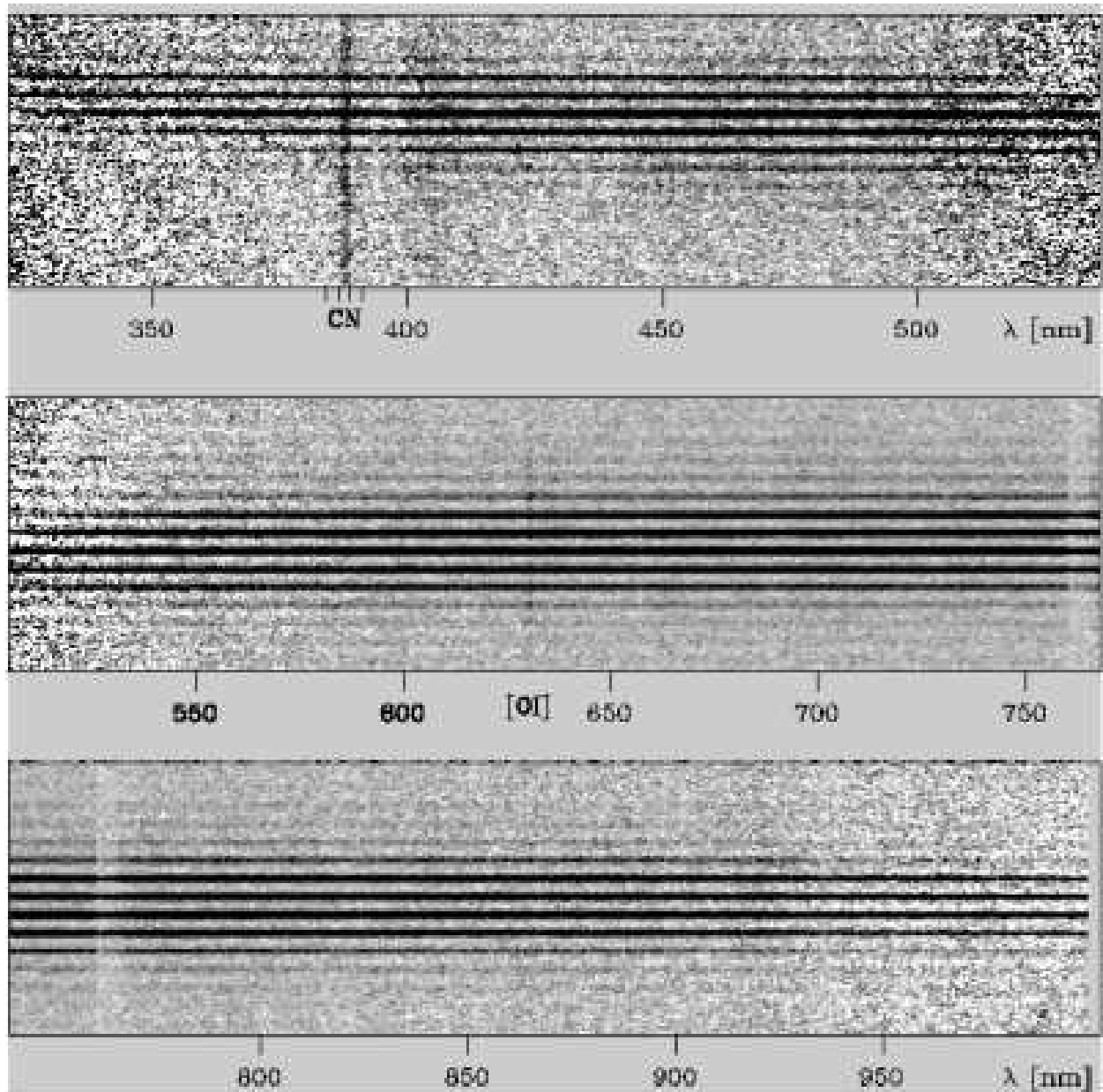


Figure 1.

Extracted SNIFS spectral datacubes in two-dimensional representation, where the columns of the integral field unit are arranged along the vertical axis. This presentation is essentially 15 long slit spectra, each 6'' long, stacked vertically. The blue spectrum is on top, the red spectrum is the center and bottom panels. The dispersion is different in blue and red spectra. The datacubes displayed here are the difference of a comet spectrum and a sky spectrum taken 5' from the comet. Therefore, no night sky lines are visible. The violet emission of CN (0-0) is strongly visible. We are also faintly detecting the C₂ emission band at 405 nm and the [OI] emission at 630 nm. The C₂ emission is too broad and faint for further analysis.

Figure 2, Hodapp et al., Deep Impact Spectro-Photometry

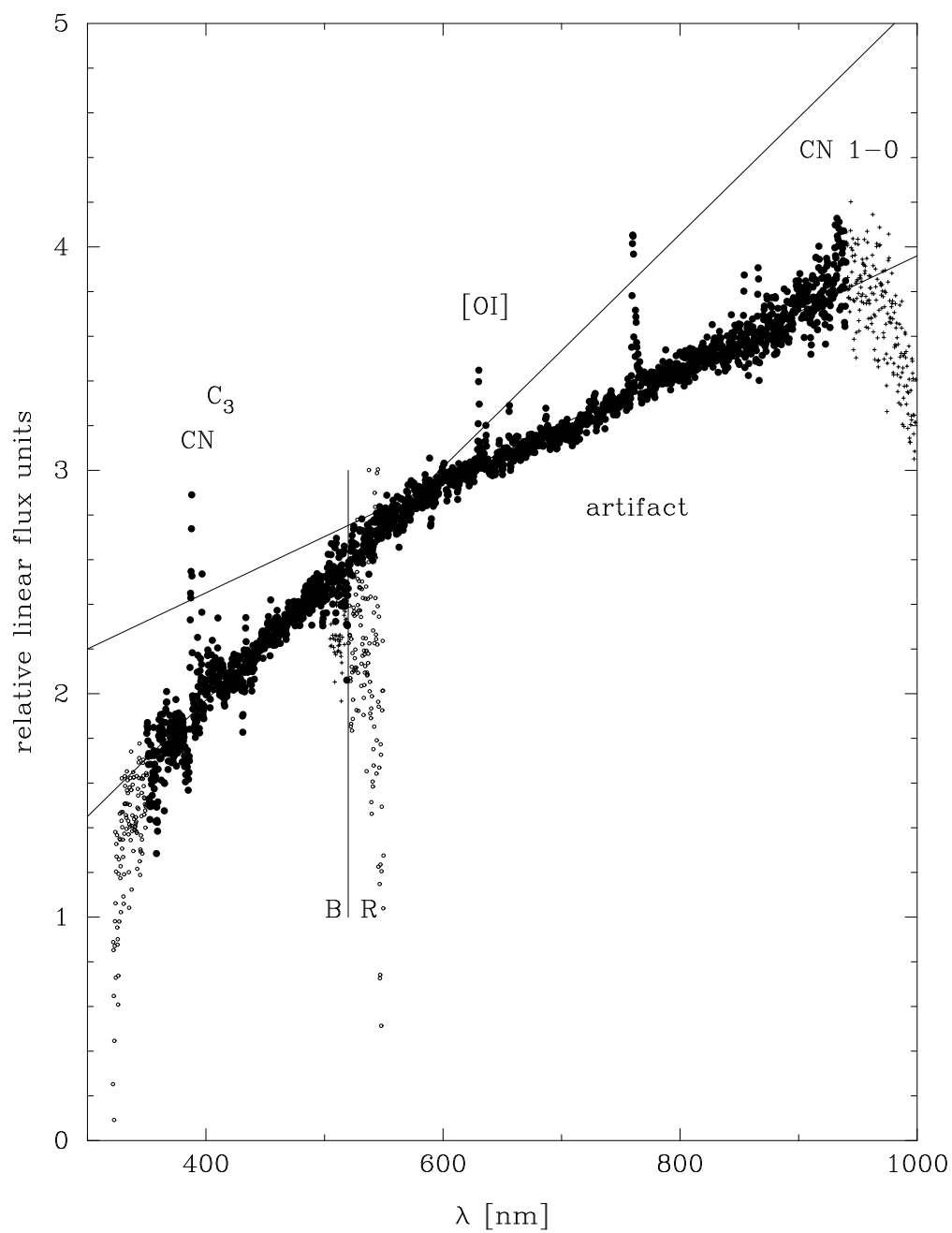


Figure 2.

Reflectivity spectrum of comet 9P/Tempel 1 after the impact, near the time of maximum brightness in a 2.4'' aperture. The spectrum is the ratio of the comet spectrum and that of solar analog star P041C and is displayed here in arbitrary linear flux units. The blue and red channel of the instrument were individually photometrically calibrated and the data match very well without further adjustment. The emission lines of CN and [OI] are clearly visible, and the C₃ band is faintly indicated. The feature at 763 nm is an artifact from the strong telluric O₂ absorption. Filled circles represent the data that are considered reliable. We also show the data at the ends of the spectral ranges of the blue spectrograph arm (small open circles) and of the red spectrograph arm (small plus signs) to illustrate that at the ends of each spectrum, the calibration was not reliable and why these data have not been included in the analysis. The boundary between where the blue vs. red data were used is at 520 nm and this boundary is indicated in the Figure. This boundary does not coincide with the change in slope of the spectrum. Below 580 nm, the normalized slope between 350 nm and 580 nm is 22.6%, between 580 nm and 940 nm, the normalized slope is 7.5%.

Figure 3, Hodapp et al., Deep Impact Spectro-Photometry

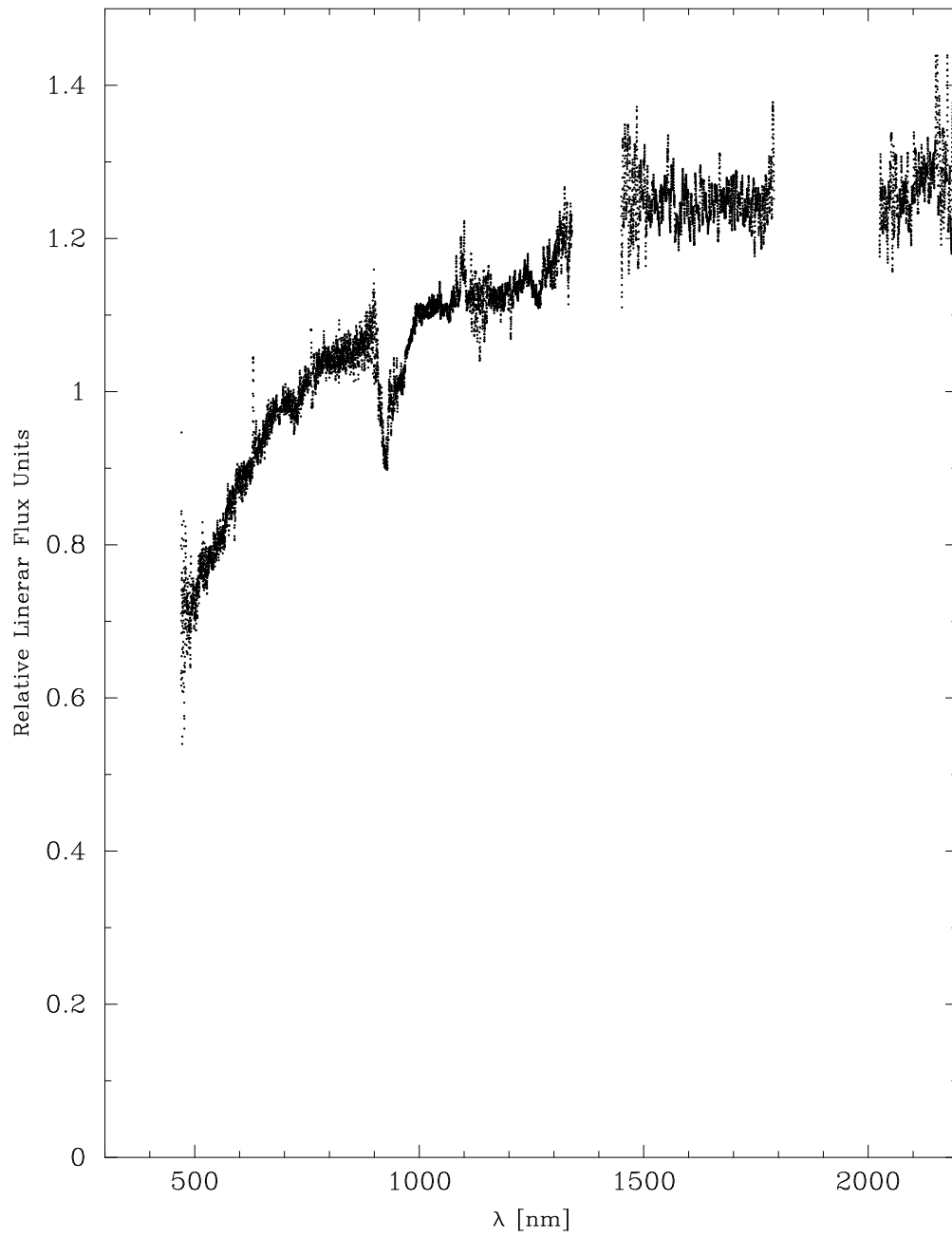


Figure 3.

Reflectivity spectrum in relative flux units, obtained with the 3-channel VNIRIS spectrograph at the Lick Observatory 3 m telescope. The spectrum covers the wavelength range from 500 nm to 2200 nm. The integration time was 12 min, centered at 6:42 UT, 50 min after the impact at the time of maximum brightness of the impact generated ejecta cloud. While this spectrum shows a poorly corrected atmospheric absorption feature at 920 nm this feature is clearly distinct from the 950 - 1000 nm feature seen in Fig. 2. Therefore, both features are artifacts. The spectrum confirms the steeper reflectivity spectrum at shorter wavelengths compared to the longer wavelengths.

Figure 4, Hodapp et al., Deep Impact Spectro-Photometry

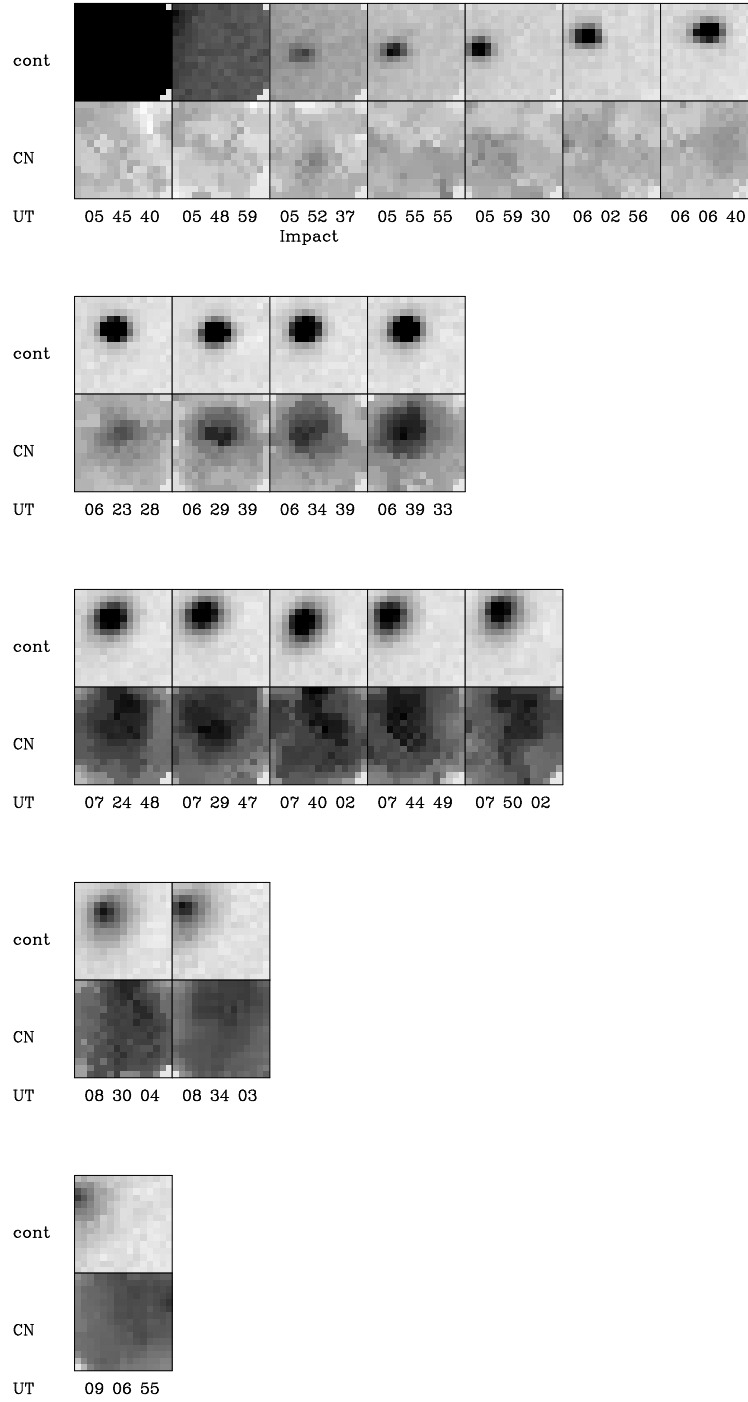


Figure 4.

The sequence of extracted, continuum-subtracted CN images during the night of the Deep Impact event. The top two left frames were taken prior to impact under twilight conditions, so the continuum image appears very dark. In those two images, the comet nucleus was located in the upper left corner of the field of view. The third image was exposed during the impact time. The weak peak found in this image is considered spurious. The gaps between groups of images indicate time when no comet data were taken because of other observing tasks such as sky fields and standard stars. CN emission centered on the comet nucleus begins to be visible about one half hour after impact, in the first frame of the second set of data. The CN emission then rapidly increases in intensity and expands spatially. About two hours after impact, the added CN emission fills the whole field of view and the average flux levels are clearly higher than before the impact. This is quantitatively displayed in the lightcurves in Fig. 6.

Figure 5, Hodapp et al., Deep Impact Spectro-Photometry

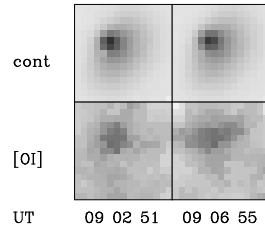
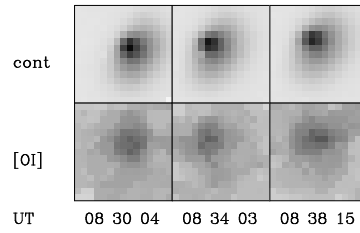
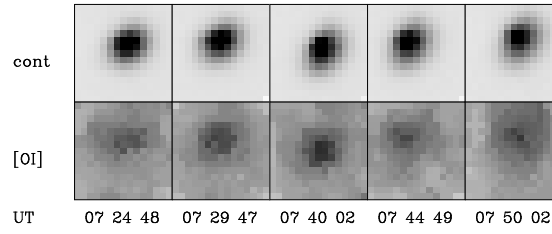
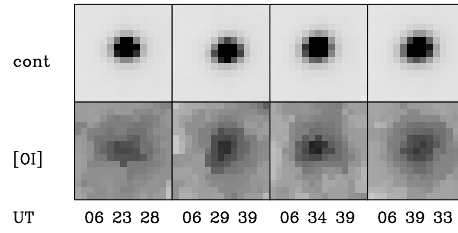
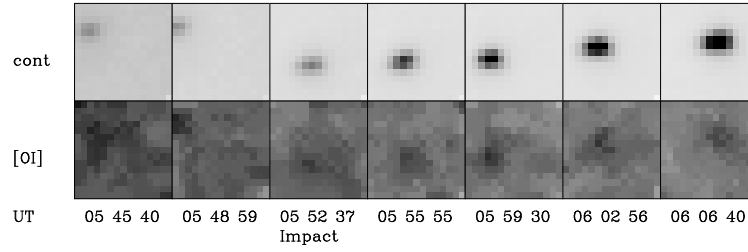


Figure 5.

The sequence of extracted, continuum-subtracted [OI] ($\lambda = 630$ nm) images during the night of the Deep Impact. In the first two images the comet nucleus was located in the upper left corner of the field of view. The third image was exposed during the impact time. The gaps between groups of images indicate time when no comet data were taken because of other observing tasks such as sky fields and standard stars. There is a uniformly distributed component of [OI] emission from night-sky emission. This component is subtracted out in the sky-subtracted aperture photometry shown in Fig. 5. The $2.8''$ diameter aperture photometry shows a rapid rise of the [OI] emission centered on the comet nucleus.

Figure 6, Hodapp et al., Deep Impact Spectro-Photometry

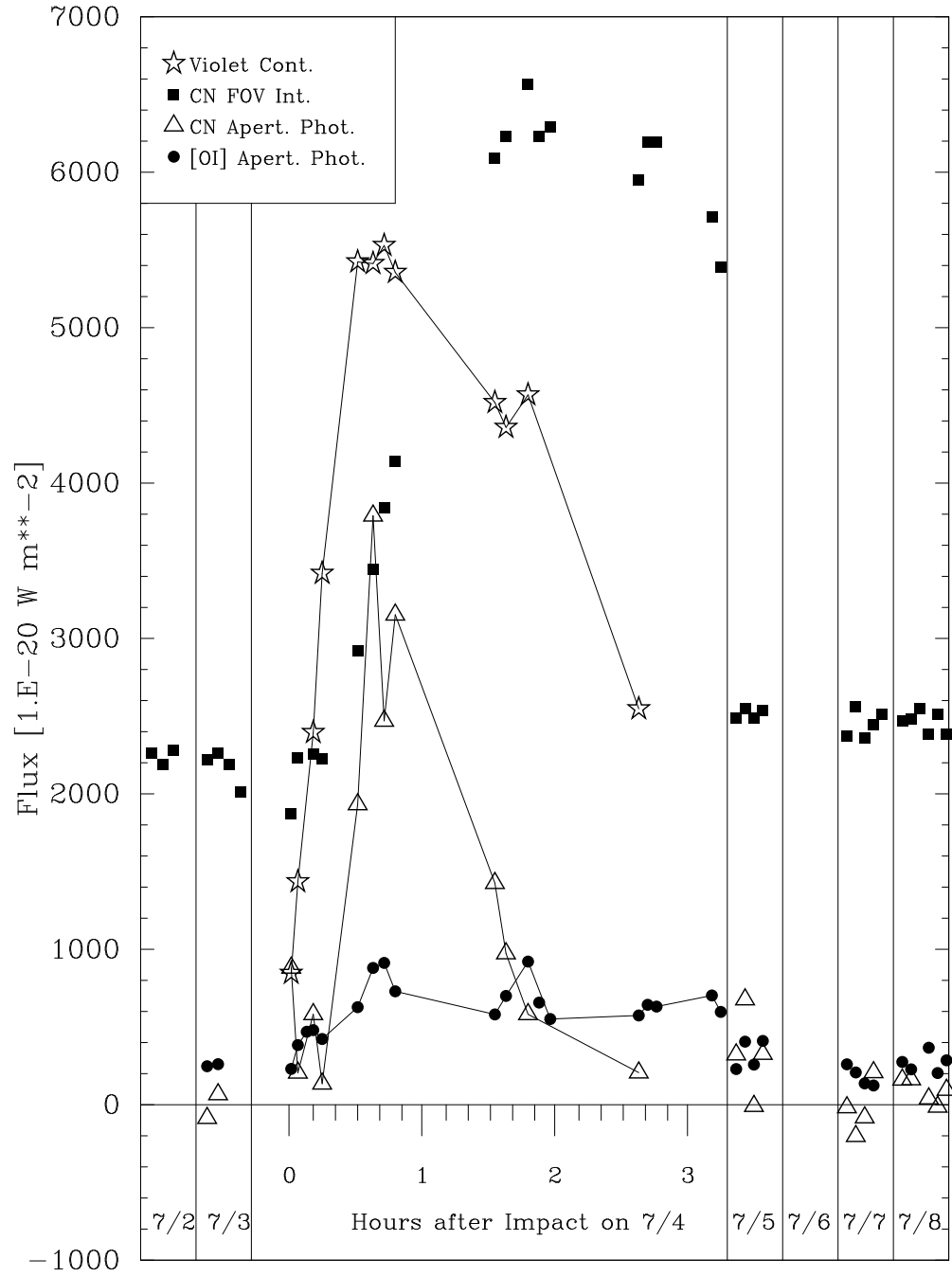


Figure 6.

This figure summarizes the photometry of comet 9P/Tempel 1 in broad bandpasses and in narrow bandpasses centered on the violet CN band and the [OI] emission features. The central panel of this figure are lightcurves obtained on July 4, 2005, UT, time is indicated in hours after the time of impact of the Deep Impact probe. The narrower panels to the right and left show individual measurements taken in the nights prior (July 2 and 3, UT) and after the impact (July 5,7,and 8). No data were obtained on July 6 due to bad weather. These data are shown in the correct sequence, but without a specific time scale on the horizontal axis, since we did not expect, nor observe, changes on timescales of less than one hour in those nights.

Several measurements are plotted here: Open triangles are aperture photometry on CN-images. Solid squares are the average CN-fluxes over the full field of $6'' \times 6''$ corresponding to $3870 \text{ km} \times 3870 \text{ km}$ at the comet. The average fluxes over the field of view (solid squares). have been scaled to an area corresponding to the $2.8''$ diameter aperture used for the gas emission aperture photometry, to help with a direct comparison of the fluxes. Filled circles are aperture photometry on [OI] images. Open stars are 350-400 nm integrated images dominated by scattered continuum, measured in $2.4''$ apertures; these measurements have been scaled by a factor of $1/50$ for comparison with the line emission fluxes. The signal is given in units of 10^{-20} Wm^{-2} , based on the SNIFS instrument absolute calibration and standard Mauna Kea extinction. We estimate the systematic uncertainty of this value to be about 10%.

Figure 7a, Hodapp et al., Deep Impact Spectro-Photometry

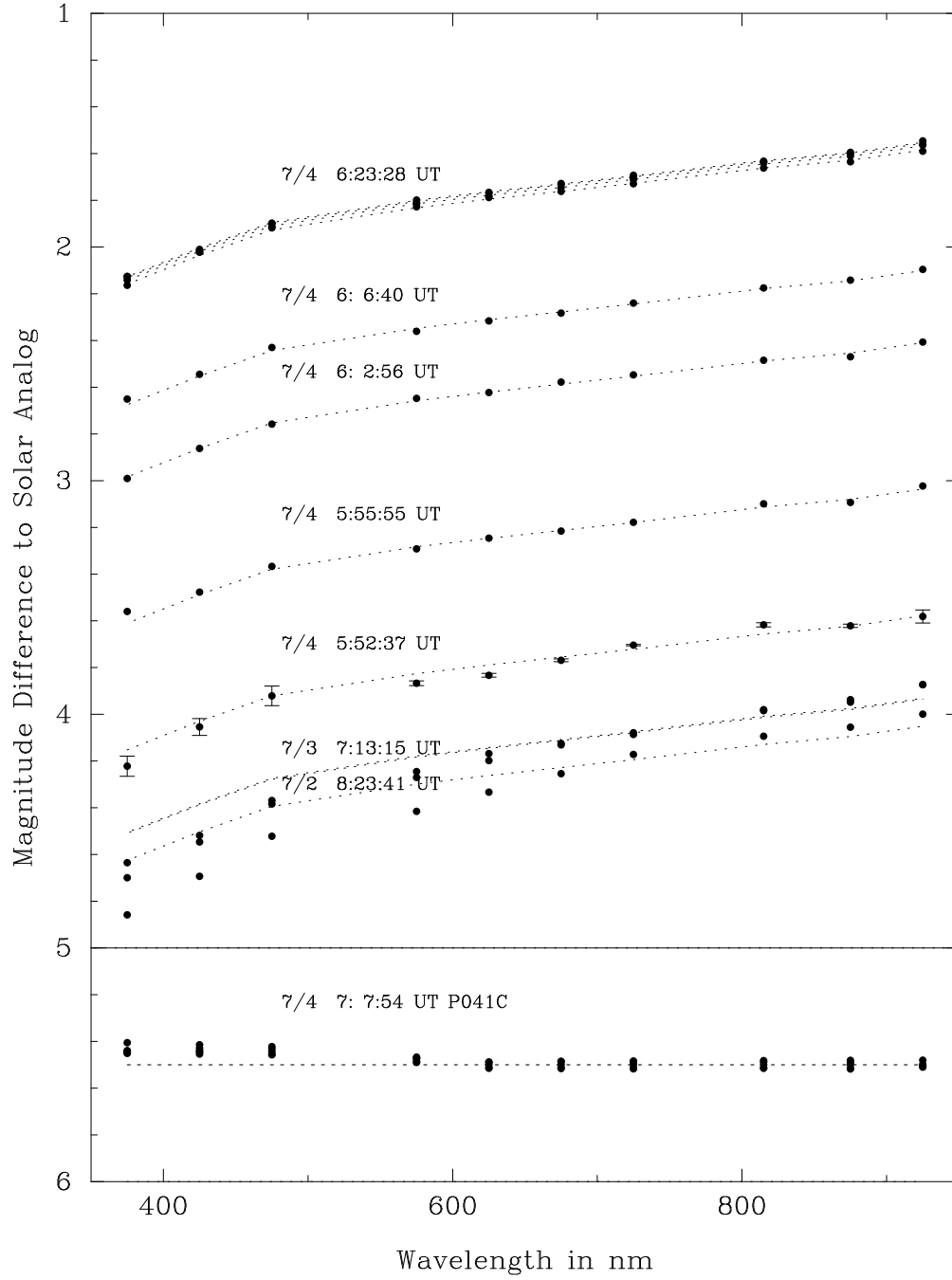


Figure 7 a.

The synthetic bandpass photometric measurements taken at different times are plotted against wavelength. All data are normalized to a solar spectrum by subtracting the data of solar analog star P041C and the appropriate flux correction. The lower panel shows the measurements of P041C on 7/4. The deviations from a constant signal are consistent with the flux corrections for these stars. In the middle panel, the comet measurements for 7/2 (shifted down for clarity) and then for 7/3 are presented. Then we plot the data taken in the first hour after impact on 7/4 without additional shifts so that the magnitude differentials represent the true lightcurve of the impact event.. Even the first frame on 7/4 (taken during impact) is brighter than 7/3. In the 2.4'' (1550 km) aperture used here for photometry, the brightness reaches a plateau about one half hour after impact. These measurements about one half hour after impact are the highest signal-to-noise data obtained on the comet and represent the state of the comet dominated by impact-generated ejecta. The average of these measurements is the “post-impact-maximum” flux distribution (dotted line) that is fitted to the other comet measurements. The measurements prior to impact show a redder continuum than the data dominated by impact generated ejecta. In other words, the impact-generated material had a bluer reflectivity spectrum than the material released by the comet under normal conditions.

Figure 7b, Hodapp et al., Deep Impact Spectro-Photometry

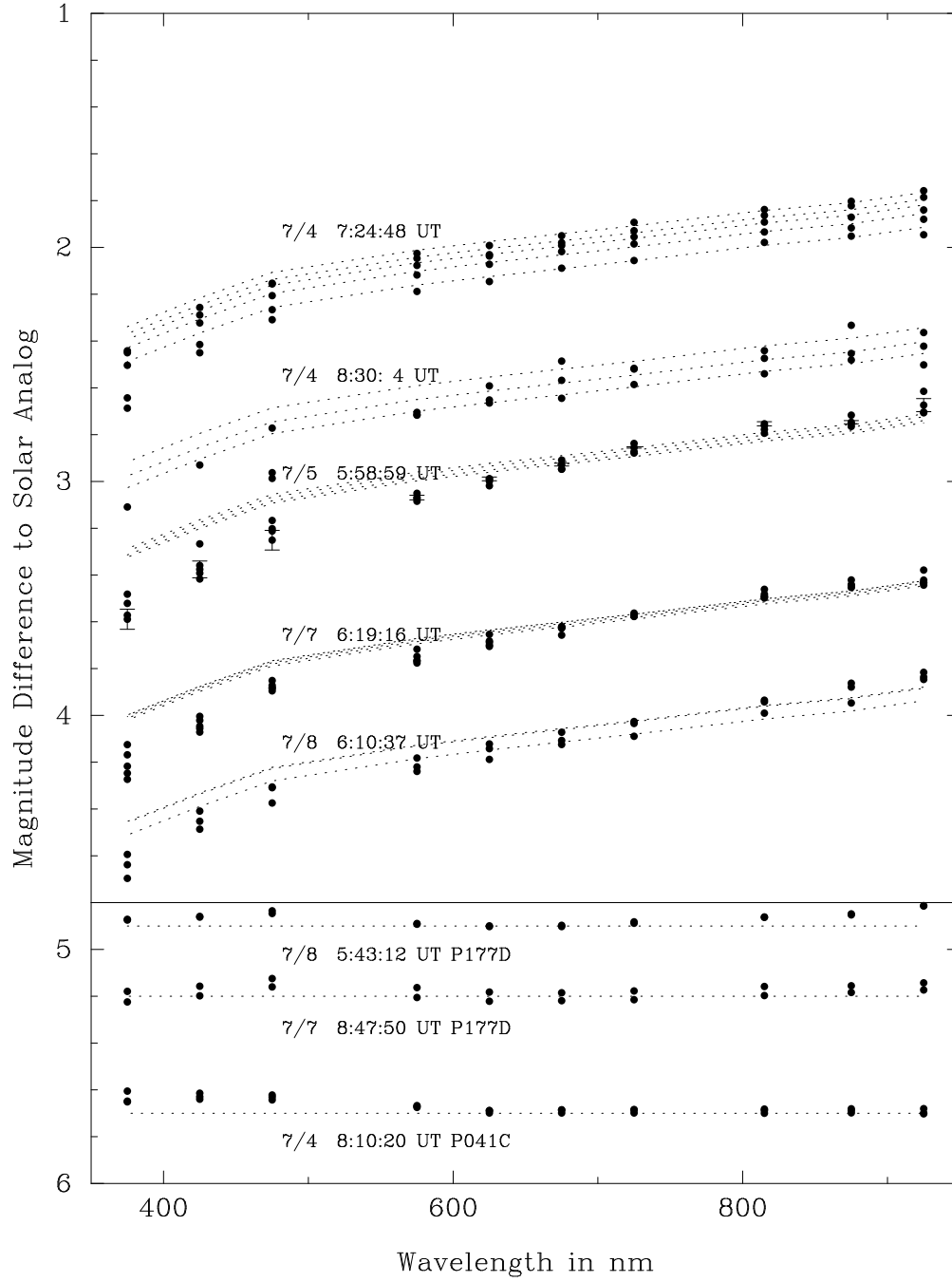


Figure 7 b.

The synthetic bandpass photometric measurements taken at different times are plotted against wavelength. All data are normalized to a solar spectrum by subtracting the data of solar analog star P041C and the appropriate flux correction. The lower panel shows the measurements of P041C on 7/4 and of another solar analog star, P177D, on 7/7 and 7/8. The deviations from a constant signal are consistent with the flux corrections for these stars. The top panel shows the comet measurements (shifted for clarity) after the lightcurve maximum on 7/4 and in the nights following the impact. After maximum brightness, the color of the comet returned to the redder continuum that was observed prior to the impact.